Huang, Ting *et al*. (2019) ***Géotechnique Letters*** **9**, 1–8, https://doi.org/10.1680/jgele.19.00028

Drained response of rigid piles in sand under an inclined tensile load

TING HUANG*, CONLETH O'LOUGHLIN†, CHRISTOPHE GAUDIN†, YINGHUI TIAN‡ and TING LU†

The response of rigid piles in sand to an inclined tensile load is poorly documented and understood, particularly when the load is cyclic. This is becoming relevant for floating marine renewable energy devices such as wave energy converters and floating wind turbines. This paper considers centrifuge data for rigid piles in dense sand subjected to drained monotonic and cyclic loading at various inclinations. The data strongly advocate (in dense sand) the avoidance of load inclinations higher than about 60° (to the horizontal) as cyclic loading significantly deteriorates pile capacity, whereas at lower (flatter) load inclinations, there are potential benefits from cyclic densification that improve pile capacity.

KEYWORDS: model tests; offshore engineering; piles & piling

NOTATION

C_c	coefficient of curvature
C_u	coefficient of uniformity
D	pile diameter
D_r	relative density
d_{50}	mean particle size
F	pile load
$F_{c,max}$	maximum cyclic load
$F_{c,min}$	minimum cyclic load
F_m	monotonic pile capacity
G_s	specific gravity
H	horizontal capacity component
L	pile length
m	mass
N	cycle number
q_c	cone tip resistance
R_{max}	maximum roughness
t	pile wall thickness
V	vertical capacity component
z	depth
Δ	pile head displacement
δ	interface friction angle
ζ_b	cyclic load magnitude
ζ_c	cyclic load symmetry
θ	load inclination
ρ_{max}	maximum dry density
ρ_{min}	minimum dry density
ϕ'_{cs}	critical state friction angle

INTRODUCTION

Offshore wave energy converters (WECs) include point absorbers that are typically submerged buoyant bodies that produce electricity through the extension of a power take off on the mooring lines. Under normal operating conditions, when the WEC is producing power, WEC motion produces extension of the power take off, creating a cyclic mooring line force that is transferred to the foundation. WEC foundations are also required to withstand the loading associated with extreme events, during which the WEC will not be producing power, but is in 'survival mode'. This extreme load is of a much higher magnitude than the typical operating load, and is dynamic in nature.

As shown in Fig. 1(a), a submerged WEC may be connected to a pile foundation in the seabed through a primary, quasi-vertical taut mooring. One option for dealing with the extreme loading event for such a mooring configuration is the use of secondary slack moorings. Under normal operating conditions, the reaction force required for power output is provided by the pile foundation on the primary mooring. The primary mooring is disconnected either before or during extreme loads (e.g. by introducing a fuse into the primary mooring), allowing the WEC to raise to the water surface. The extreme loads acting on the WEC are then shared across a number of secondary moorings that are connected to either alternate or adjacent (primary mooring) foundations. This requires that the secondary mooring arrives at the seabed either horizontally or at an inclination, rather than vertically as is the case for the primary mooring.

An alternative mooring configuration is the use of three inclined taut moorings with a power take-off on each mooring line, as shown in Fig. 1(b). In this configuration the moorings transfer both the operational and extreme loads, such that the foundations at the end of each mooring must be designed to resist both classes of load. This mooring configuration is also used for offshore floating wind turbines – for example, the Hywind demonstration project (Skaare *et al*., 2015).

Either mooring configuration involves tensile, inclined cyclic loading of the foundation. There is little experience of how piles perform under such loading, particularly in the sandy seabeds where the majority of commercial WEC developments are expected to be sited. The contribution of this paper is experimental evidence that quantifies the response of a rigid pile foundation in dense sand under inclined tensile monotonic and cyclic drained loading.

EXPERIMENTAL DETAILS

Model piles

The experiments were conducted in a geotechnical centrifuge at 100***g*** using aluminium closed-end piles with length,

Manuscript received 1 March 2019; first decision 3 July 2019; accepted 4 July 2019.

*College of Harbor, Coastal and Offshore Engineering, Hohai University, Nanjing, China.
†Centre for Offshore Foundation Systems, Perth, WA, Australia.
‡Melbourne School of Engineering, The University of Melbourne, Melbourne, VIC, Australia. Formerly Centre for Offshore Foundation Systems, Perth, WA, Australia.

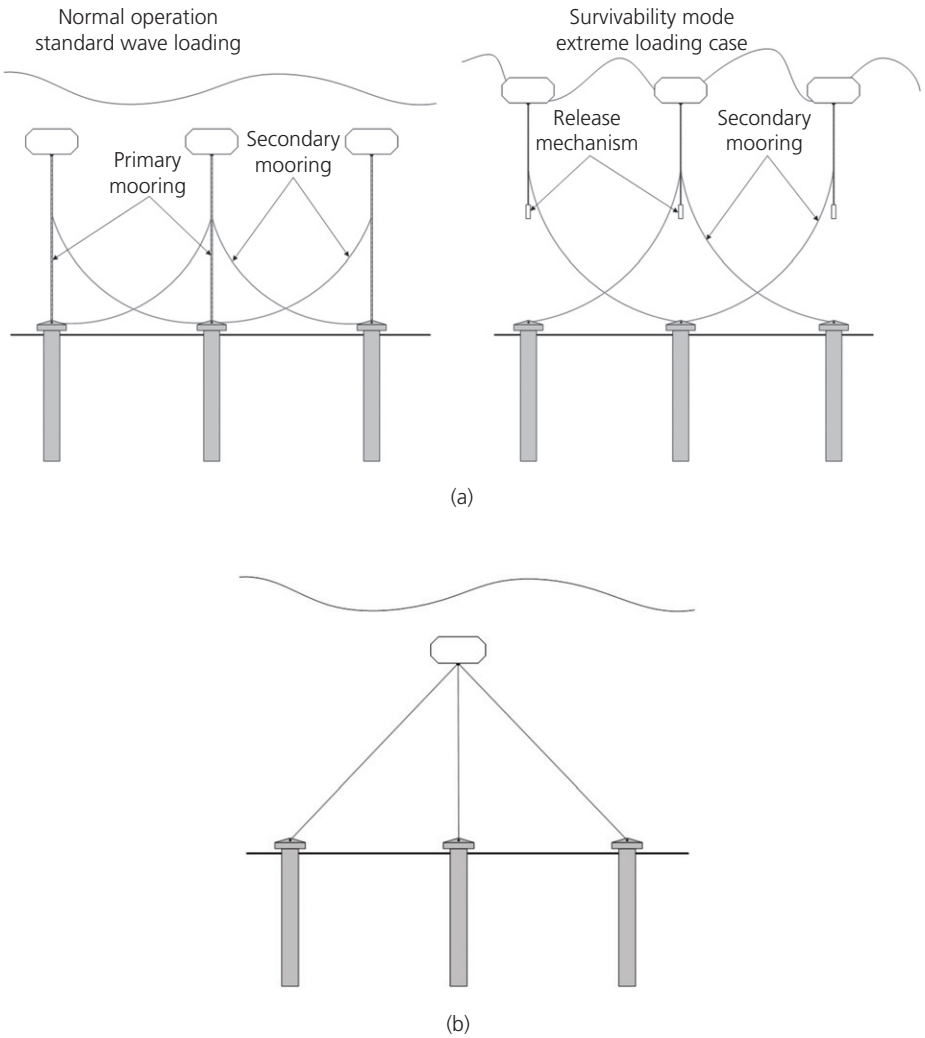

Fig. 1. Example mooring configurations for point absorber WECs: (a) single vertical primary mooring under normal operation and slack secondary moorings under extreme conditions; (b) three inclined taut mooring lines

$L = 155$ mm, diameter, $D = 22$ mm, wall thickness, $t = 4$ mm (see Fig. 2) and mass, $m = 136$ g. The model piles are sufficiently stiff for the response to be considered rigid (Poulos & Hull, 1989). The surface of each pile was either anodised or bead blasted to give (respectively) an average relative roughness, $R_{max}/d_{50} = 0{\cdot}04$ and $0{\cdot}30$, such that the piles could be categorised as either (almost) smooth or rough (Lings & Dietz, 2005).

Soil samples

Eleven soil samples were prepared in containers measuring 650×390 mm in plan with a depth of 325 mm, using a fine-to-medium sub-angular silica sand with properties as listed in Table 1. The samples were first prepared by air pluviation with the piles 'pre-located' in the container (using very fine suspension wires), before saturation from the sample base. Saturation was deemed complete when a layer of free water developed above the sample surface (and flooded the hollow piles by way of a vent hole at the top of each pile). The relative density of the samples was $D_r = 75\%$, as assessed from global measurements of mass and volume of control samples with no embedded piles. Pre-locating the piles in each sample was undertaken to avoid potential variations in the soil state surrounding each pile due to installation effects. Five piles were located in each sample, with the sand surface flush with the pile head and arranged spatially to minimise interaction and boundary effects, considering the load inclination for each pile (e.g. see Figs 3 and 5).

Cone penetration tests (using a 7 mm diameter model cone penetrometer) were conducted in each sample before the pile tests. Profiles of cone tip resistance, q_c, with depth, z are provided in Fig. 4, which shows that q_c was consistent within $\pm 11\%$ across all 11 samples, confirming that the sample preparation procedure resulted in repeatable samples.

Procedure

An electrical actuator was used to load the piles, either in displacement control for monotonic loading, or in load control for cyclic loading. Loading was achieved using a steel wire that was connected to a point 22 mm above the pile head and the vertical axis of the actuator. For the vertically loaded piles, the actuator was positioned such that its vertical axis was located directly above the centreline of the pile (Fig. 5(a)). Variations in the load inclination, θ (measured relative to the horizontal), were achieved by pre-setting the vertical and horizontal distance between a pulley located at the base of the actuator and the pile head (Fig. 5(b)). Pile capacity was measured using a load cell located in series with the mooring line, and the displacement of the line was measured using the encoder on the vertical axis of the actuator.

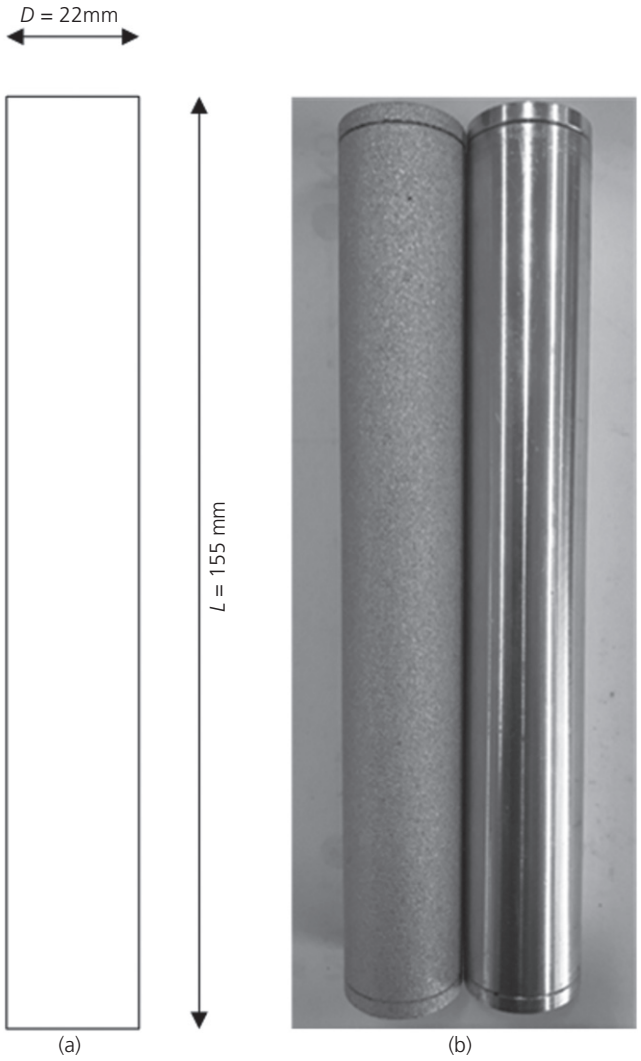

Fig. 2. Model piles: (a) schematic; (b) photographs (left: rough pile, right: smooth pile)

Table 1. Properties of the silica sand used in this study

Property	Value
Specific gravity, G_s	2·67
Median particle size, d_{50}	0·18 mm
Coefficient of uniformity, C_u	1·67
Coefficient of curvature, C_c	1·02
Minimum dry density, ρ_{min}	1497 kg/m^3
Maximum dry density, ρ_{max}	1774 kg/m^3
Critical state friction angle, ϕ'_{cs}	31·6° (triaxial)

After Chow *et al.* (2018)

A displacement rate of 0·1 mm/s was adopted for the monotonic tests, whereas the cyclic tests involved 1000 one-way sinusoidal loading cycles at a frequency of 0·5 Hz, such that in either case, the response was drained. The cyclic load magnitude and symmetry was described using the parameters ζ_b and $\hat{\zeta}_c$, respectively

$$\zeta_b = \frac{F_{c,max}}{F_m}, \quad \hat{\zeta}_c = \frac{F_{c,min}}{F_m} \tag{1}$$

where $F_{c,min}$ and $F_{c,max}$ are the minimum and maximum cyclic loads in a load cycle and F_m is the monotonic capacity. These cyclic loading parameters are similar to those

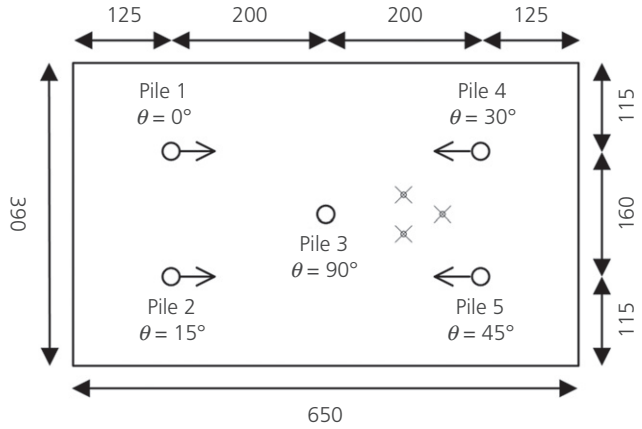

Fig. 3. Test layout in sample 4 (dimensions in mm)

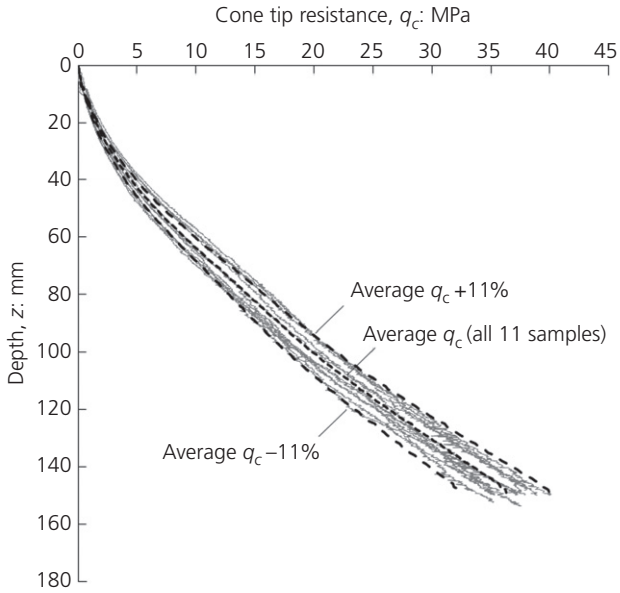

Fig. 4. Depth profiles of cone tip resistance

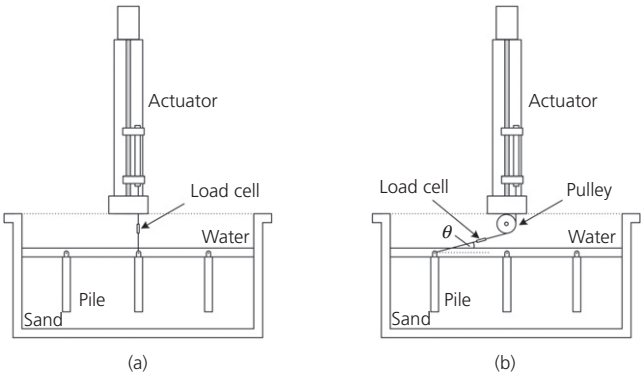

Fig. 5. Pile loading arrangement: (a) vertical loading; (b) inclined and horizontal loading

introduced by LeBlanc *et al.* (2010), but with $\hat{\zeta}_c$ quantified relative to the monotonic capacity, F_m, rather than to the maximum cyclic load, $F_{c,max}$. In the cyclic tests that did not result in pile failure, a post-cyclic loading monotonic test was conducted to quantify the change in monotonic capacity due to cyclic loading.

PROGRAMME, RESULTS AND DISCUSSION

The experimental programme is summarised in Table 2 and comprises 14 monotonic tests (M1–M14) and 12 cyclic tests (C1–C12). The load inclination was varied in 15° intervals from 0 to 90°, such that seven different load inclinations were considered. Monotonic tests were conducted on both rough and smooth piles, whereas cyclic tests were conducted only on rough piles. All cyclic tests involved one-way loading with $\zeta_c = 0{\cdot}1$, whereas the cyclic load magnitude was $\zeta_b = 0{\cdot}5$ for all load inclinations, with a limited number of additional tests at $\theta = 0$ and 90° employing higher and lower cyclic load magnitudes ($\zeta_b = 0{\cdot}3$–$0{\cdot}9$), motivated by the response measured at $\zeta_b = 0{\cdot}5$.

Monotonic tests

Typical results from the monotonic tests are provided in Fig. 6 for both the rough and smooth piles, at load inclinations, $\theta = 90$, 45 and 0°. Evidently, interface roughness (and the associated dilation) has a very significant influence on (*a*) vertical capacity (Fig. 6(a)) as the monotonic pile capacity, F_m (i.e. the maximum value of the pile load, F) for the rough pile is almost three times that of the smooth pile and (*b*) post-peak response with the rough pile exhibiting significant softening behaviour. This difference is much less significant at $\theta = 45°$ (Fig. 6(b)) and not discernible for $\theta = 0°$ (Fig. 6(c)). Figure 6 also indicates that for this pile aspect ratio ($L/D = 7$), F_m for horizontal loading is twice that for vertical loading when the interface is rough, increasing to a factor of 6·2 when the interface is smooth. The post-peak response for both the smooth and rough interfaces is characterised by load oscillations for $\theta = 45$ and 90°. This is attributed to the progressive infilling of voids that form around the pile when the loading is non-vertical, similar to observations from tensile loading tests on plates and pipes buried in sand (e.g. Cheuk *et al.*, 2008; O'Loughlin & Barron, 2012). Much larger displacements are required to mobilise the peak pile capacity as θ reduces, which is consistent with the higher stiffness for vertical loading than for horizontal loading prescribed by existing calculation methods (e.g. API, 2011).

Figure 7 shows the evolution of pile capacity with load inclination. Capacity reduces as the load inclination becomes more vertical, reflecting the transition in failure mechanism from a combination of passive and active soil resistance along the pile under pure horizontal loading, to pure shearing at the pile–soil interface under vertical loading. Under low-load inclinations the smooth and rough piles exhibit very similar capacity as the mechanism involves shearing within the soil, whereas at high-load inclinations the capacity of the smooth and rough piles differ significantly as the mechanism involves more shearing at the pile–soil interface. Practically, the effect of interface roughness is most pronounced for load inclinations between $\theta = 90$ and 45°; below 45° the difference in capacity for the rough and smooth piles reduces from 15% at $\theta = 45°$ to 5% at $\theta = 0°$.

Additional insights into the influence of the load inclination can be obtained by plotting the vertical (V) and horizontal (H) components of the inclined capacity in a V–H interaction diagram, as shown in Fig. 8. As the load inclination reduces from $\theta = 90$ to 0°, the vertical capacity component initially reduces (at $\theta = 75°$) and then increases up to $\theta = 60°$ (rough pile) and $\theta = 45°$ (smooth pile). Although the initial reduction in the vertical capacity component at $\theta = 75°$ does not correspond to a reduction in pile capacity (see Fig. 7), there is no enhancement of pile capacity, indicating that passive resistance has not been mobilised at this rather steep load inclination. As the load inclination further reduces, passive resistance is mobilised, leading to pile capacity increases that are more significant for the smooth pile than the rough pile. At lower load inclinations the vertical capacity component reduces with the transition to the rigid pile rotation mechanism associated with laterally loaded rigid piles.

Figure 8 also shows the theoretical interactions for the rough and smooth pile, assuming no coupling between the vertical and horizontal capacity components – that is, the

Table 2. Test programme

Test ID	Pile interface	Load inclination, θ: °	Test type	Cyclic load magnitude, ζ_b	Post-cyclic monotonic loading
M1	Rough	0	Monotonic	—	—
M2		15		—	—
M3		30		—	—
M4		45		—	—
M5		60		—	—
M6		75		—	—
M7		90		—	—
M8	Smooth	0		—	—
M9		15		—	—
M10		30		—	—
M11		45		—	—
M12		60		—	—
M13		75		—	—
M14		90		—	—
C1	Rough	0	Cyclic	0·5	Y
C2		0		0·3	
C3		0		0·7	
C4		0		0·9	
C5		15		0·5	
C6		30		0·5	
C7		45		0·5	
C8		60		0·5	
C9		75		0·5	
C10		90		0·5	N
C11		90		0·25, 0·5	
C12		90		0·3	Y

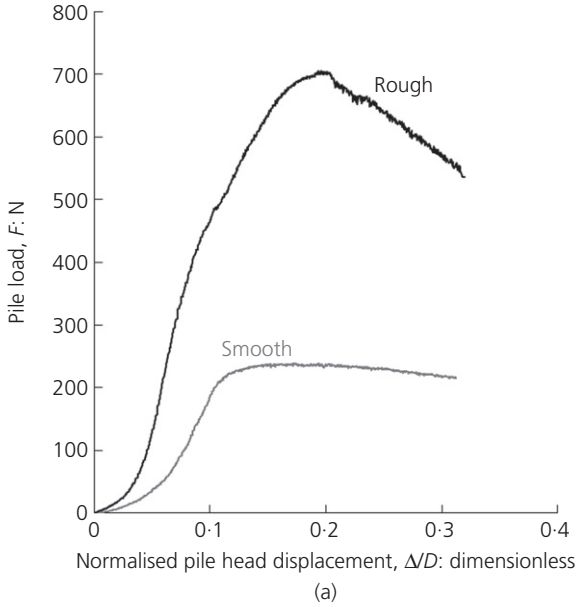

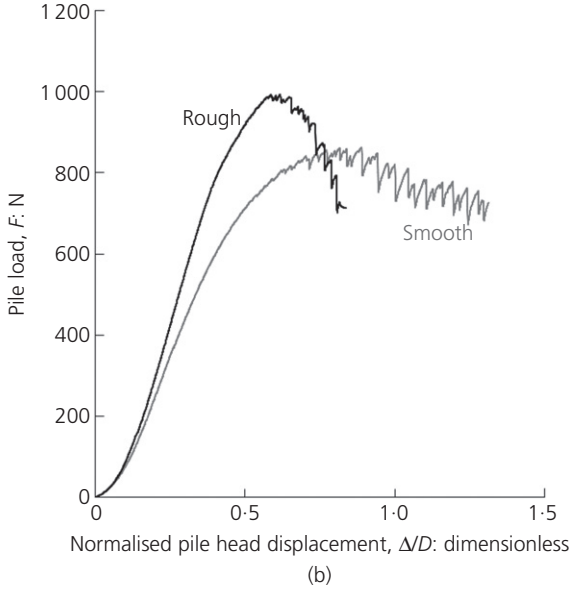

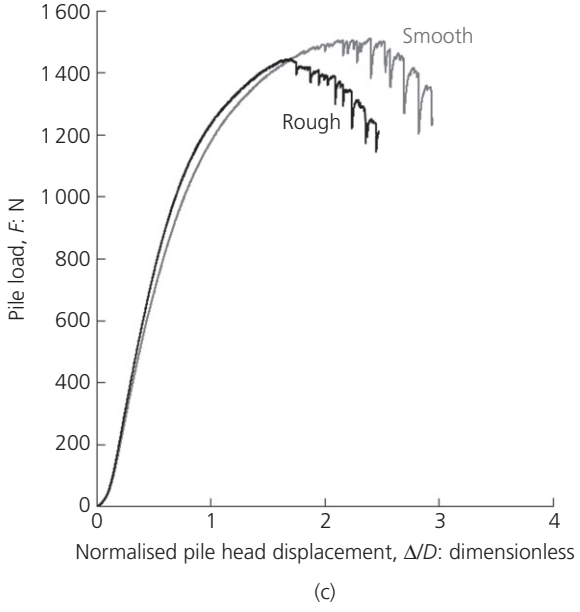

Fig. 6. Monotonic load–displacement response: (a) vertical loading ($\theta = 90°$); (b) inclined loading (($\theta = 45°$) and (c) horizontal loading ($\theta = 0°$)

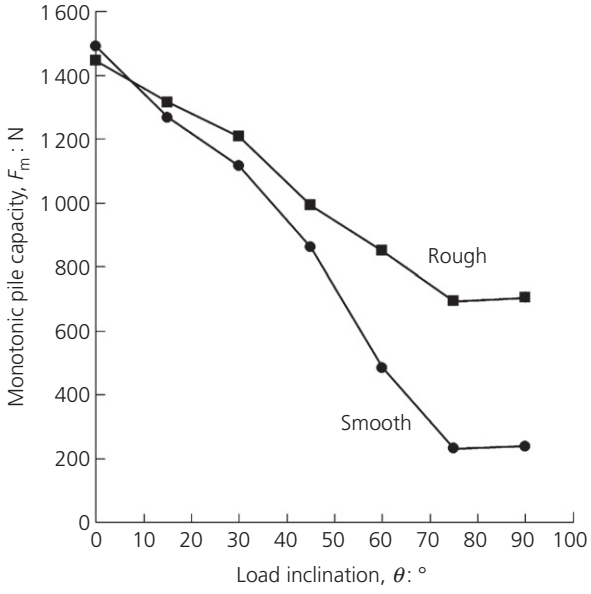

Fig. 7. Variation of pile capacity with load inclination for rough and smooth interfaces

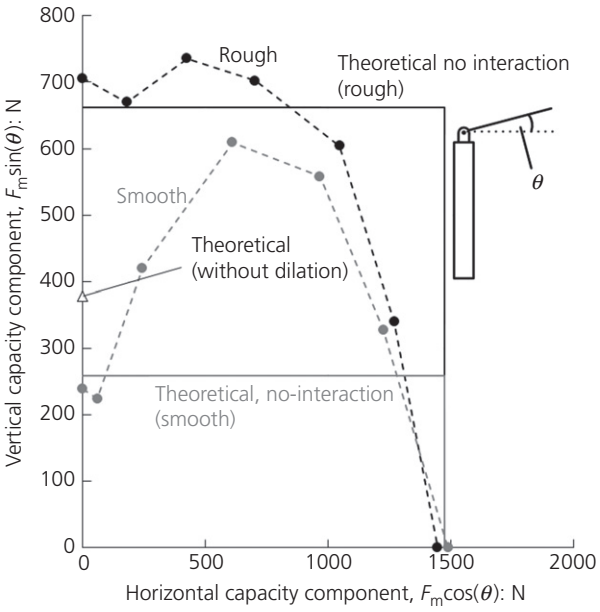

Fig. 8. Interaction of vertical and horizontal components of tensile pile capacity

shape of the interaction diagram is rectangular. While the maximum vertical capacity (at $H = 0$) is also the ultimate vertical capacity, the horizontal capacity (at $V = 0$) simply represents the maximum, but not the ultimate capacity as this depends on the load application point. Hence the interaction in Fig. 8 can only be considered valid for this pile geometry and load application point. The theoretical vertical capacity was calculated by summing the local shear stress at failure along the pile wall (Lehane *et al.*, 2005) and adopting an interface friction angle, $\delta = 40$ and 23° for the rough and smooth piles, respectively. Selection of these values was guided by the variation in interface friction angle with interface roughness reported in Lings and Dietz (2005), such that the peak friction angle for this sand (at relevant stress and density levels) was selected for the rough pile (Lehane & Liu, 2013) and an assumed interface

friction angle (based on interface roughness) was selected for the smooth pile. The choice of interface friction angles appears justified as the vertical capacity for both the smooth and rough piles is calculated reasonably well (within 8%), although the importance of accounting for dilation for the rough pile is evident from the additional calculation that ignores dilation. The theoretical horizontal capacity was calculated using the p–y approach for piles in sand (API, 2011) with a peak friction angle of 40° (i.e. as also used for the theoretical vertical capacity) and gives remarkable agreement with the measured capacity. A comparison of the experimental and theoretical interaction in Fig. 8 indicates that the no-coupling simplification would lead to an overestimation of the pile capacity for load inclinations up to about $\theta = 35°$ (by up to ~30%) for the rough pile, whereas the capacity of the smooth pile is generally underestimated by a maximum factor of about 2. It follows that calculation approaches for pile tensile capacity under an inclined load should allow for this interaction, particularly when the interface is not fully rough.

Cyclic tests

As shown in Table 2, cyclic tests were conducted on the rough piles only, at each of the seven load inclinations. Figure 9 shows the pile response to cyclic loading for horizontal and vertical loading, and for $\zeta_b = 0{\cdot}5$ and $\zeta_c = 0{\cdot}1$. Failure occurred after approximately 50 cycles under vertical loading, while the response was stable for horizontal loading over the 1000 cycles, with the post-cyclic monotonic test giving a ~10% increase in pile capacity. The evolution and magnitude of pile head displacement during cyclic loading is more evident in Fig. 9(c). Pile head displacement under vertical cycles of load is initially small at $\Delta/D \sim 0{\cdot}1$, increasing steadily over the first 50 cycles before accelerating rapidly to failure. In contrast, under horizontal load cycles the initial pile head displacement is relatively high ($\Delta/D \sim 0{\cdot}5$) but increases steadily in a quasi-stabilising manner over the 1000 cycles. These differing responses reflect the two different mechanisms for vertical and horizontal loading, with only interface friction being mobilised under vertical loading while passive and active soil resistance are mobilised during horizontal loading.

Additional vertically loaded cyclic tests with cyclic load magnitudes, $\zeta_b = 0{\cdot}25$ and 0·3 were conducted to quantify the level of pure vertical cyclic loading that could be applied without leading to failure. The results from these tests are shown in Fig. 10, where it can be seen that although both cyclic load levels did not lead to failure, the displacement response (Fig. 10(c)) was stable at $\zeta_b = 0{\cdot}25$, but was meta-stable at $\zeta_b = 0{\cdot}3$, such that the behaviour beyond the 1000 cycles would be uncertain. After the 1000 cycles at $\zeta_b = 0{\cdot}25$, the cyclic load magnitude was increased to $\zeta_b = 0{\cdot}5$, causing failure after approximately ten cycles.

Similarly, additional tests with cyclic load magnitudes, $\zeta_b = 0{\cdot}3$, 0·7 and 0·9 were used for horizontal loading in an attempt to understand the effect of low- and high-level cyclic loading on pile capacity. The results from these cyclic tests are shown in Fig. 11, and show that under horizontal cyclic loading, the response was stable up to $\zeta_b = 0{\cdot}7$, becoming meta-stable at $\zeta_b = 0{\cdot}9$.

Figure 12 quantifies the effect of this cyclic loading by comparing the monotonic capacity with and without cyclic loading. Evidently, for this pile geometry a load inclination up to $\theta = 60°$ did not detriment the pile capacity, whereas for $\theta > 60°$, cyclic loading had an extremely damaging effect, reducing the monotonic pile capacity by approximately 18% for $\theta = 75°$ at $\zeta_b = 0{\cdot}5$, increasing to a 32% reduction for $\theta = 90°$ at $\zeta_b = 0{\cdot}3$, recalling that failure occurred during

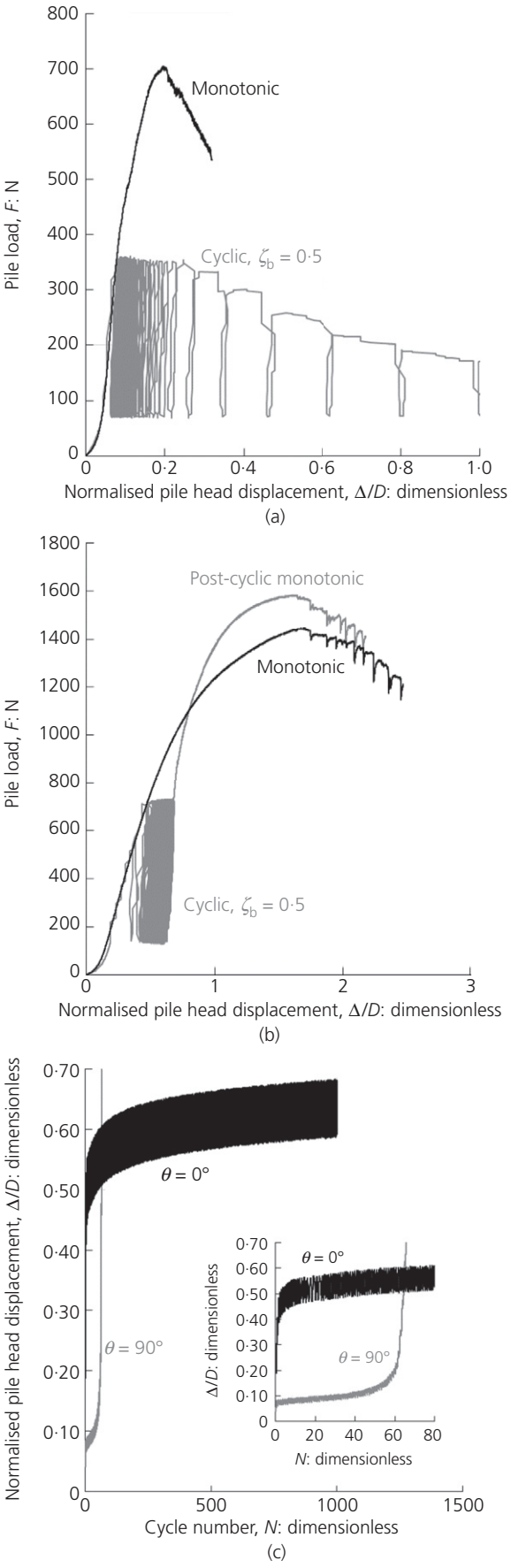

Fig. 9. Pile response during pure vertical and pure horizontal cyclic loading at a load magnitude, $\zeta_b = 0{\cdot}5$: (a) vertical loading ($\theta = 90°$); (b) horizontal loading ($\theta = 0°$) and (c) pile head displacement (in the direction of load inclination) during cyclic loading

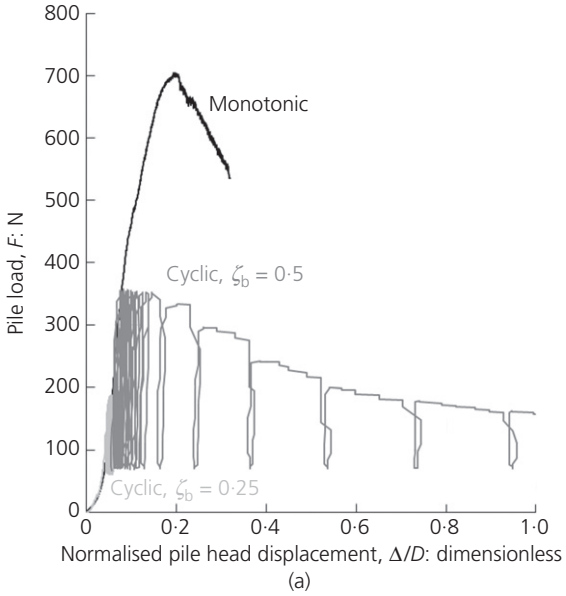

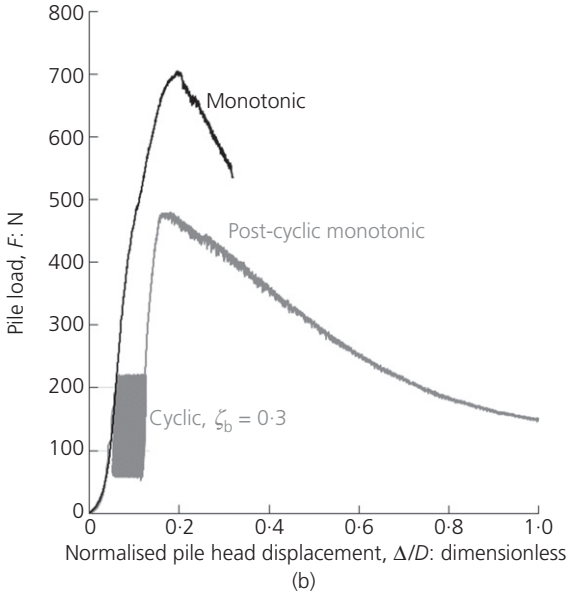

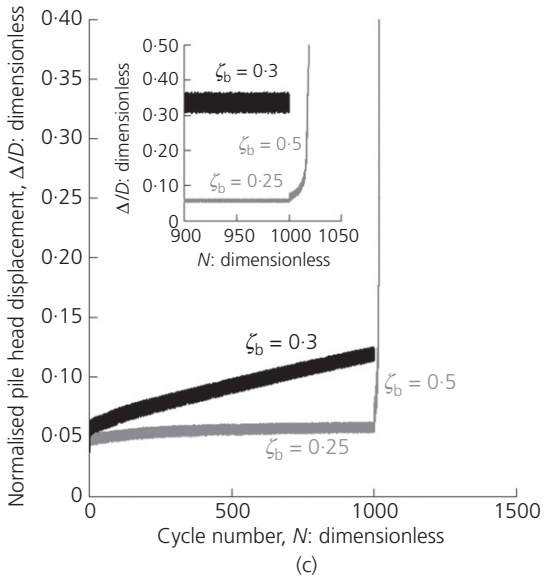

Fig. 10. Pile response during vertical cyclic loading ($\theta = 90°$) at a load magnitude: (a) $\zeta_b = 0{\cdot}25$ ($N = 1000$) followed by $\zeta_b = 0{\cdot}55$; (b) $\zeta_b = 0{\cdot}3$ and (c) pile head displacement (in the direction of load inclination) during vertical cyclic loading

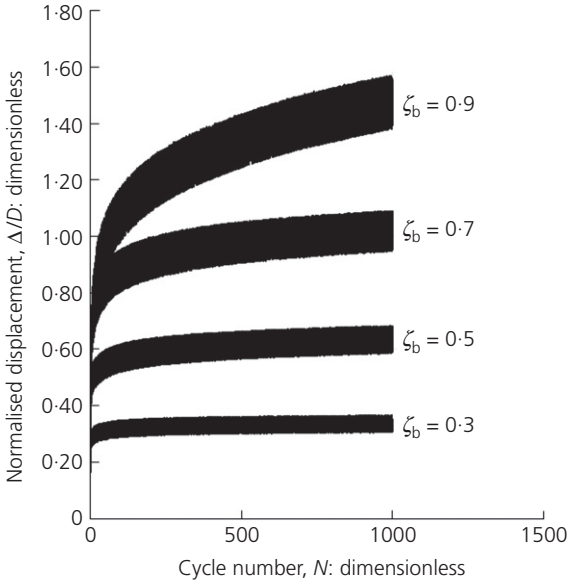

Fig. 11. Pile response during horizontal cyclic loading ($\theta = 0°$) at load magnitudes of $\zeta_b = 0{\cdot}3$, $0{\cdot}5$, $0{\cdot}7$ and $0{\cdot}9$

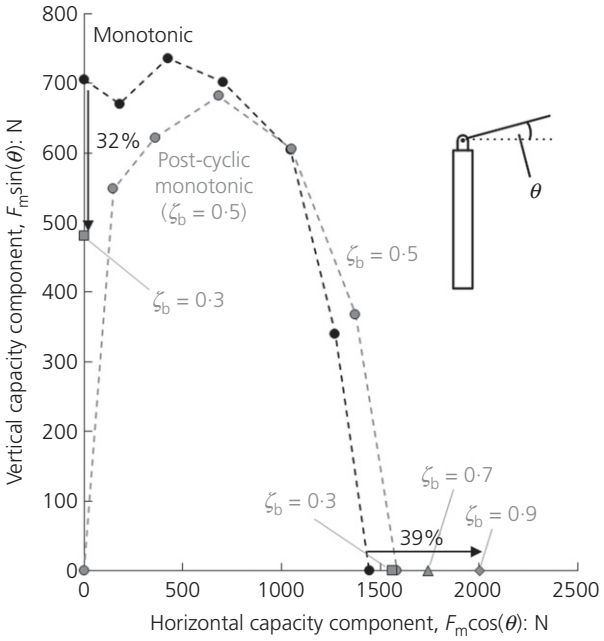

Fig. 12. Modifications to the interaction diagram after 1000 cycles of drained tensile loading

cyclic loading at $\zeta_b = 0{\cdot}5$. In contrast, horizontal cyclic loading led to increases in pile capacity between ~8 and 39% as ζ_b increased from 0·3 to 0·9. Such increases are attributed to cyclic densification and are consistent with observations from tests on suction caissons and monopiles in sand, but where the horizontal load was at a significant eccentricity from the foundation (e.g. Nicolai *et al.*, 2017; Zhu *et al.*, 2018).

CONCLUDING REMARKS

The aforementioned results provide guidance for the mooring design of a WEC; avoiding higher mooring line inclinations allows the pile design to be driven by monotonic conditions, with potential benefits of cyclic densification

leading to higher safety margins over the life of the facility. In contrast, a mooring configuration that involves near-vertical moorings may require significant degradation of the pile capacity due to the damaging effect of cyclic loading. Implications for pile design are significant. For the pile-aspect ratio adopted in this study, the mooring line inclination should be maintained below $\theta = 60°$ to avoid the cyclic degradation of pile capacity.

ACKNOWLEDGEMENTS

This work was funded by the Australian Renewable Energy Agency (ARENA) as part of ARENA's Research and Development Programme in a joint project with Carnegie Clean Energy (grant number 2015RND086). The first author received support from the Fundamental Research Funds for the Central Universities (grant number 2017B15714) and China Scholarship Council.

REFERENCES

API (American Petroleum Institute) and ISO (International Organization for Standardization) (2011). ANSI/API Specification RP 2GEO. Geotechnical and Foundation Design Considerations for Offshore Structures. Washington, DC, USA: API.

Cheuk, C. Y., White, D. J. & Bolton, M. D. 2008. Uplift mechanism of pipes buried in sand. *J. Geotech. Geoenviron. Engng.* **134**, No. 2, 154–163.

Chow, S. H., O'Loughlin, C. D., Gaudin, C. & Lieng, J. T. (2018). Drained monotonic and cyclic capacity of a dynamically installed plate anchor in sand. *Ocean Engng.* **148**, 588–601, https://doi.org/10.1016/j.oceaneng.2017.11.051.

LeBlanc, C., Houlsby, G. T. & Byrne, B. W. (2010). Response of stiff piles in sand to long-term cyclic lateral loading. *Géotechnique* **60**, No. 2, 70–90, https://doi.org/10.1680/geot.7.00196.

Lehane, B. M. & Liu, Q. B. (2013). Measurement of shearing characteristics of granular materials at low stress levels in a shear box. *Geotech. Geol. Engng.* **31**, No. 1, 329–336.

Lehane, B., Schneider, J. & Xu, X. (2005). The UWA-05 method for prediction of axial capacity of driven piles in sand. In *Proceedings of the international symposium on frontiers in offshore geotechnics* (eds S. M. Gourvenec and M. J. Cassidy), pp. 683–689. London, UK: Taylor & Francis Group.

Lings, M. L. & Dietz, M. S. (2005). The peak strength of sand-steel interfaces and the role of dilation. *Soils Found.* **45**, No. 6, 1–14.

Nicolai, G., Ibsen, L. B., O'Loughlin, C. D. & White, D. J. (2017). Quantifying the increase in lateral capacity of monopiles in dense sand due to cyclic loading. *Géotech. Lett.* **7**, No. 3, 242–252, https://doi.org/10.1680/jgele.16.00187.

O'Loughlin, C. D. & Barron, B. (2012). Capacity and keying response of plate anchors in sand. In *Proceedings of the 7th international conference on offshore site investigation and geotechnics* (eds P. Allan, J. Arthur, A. Barwise, T. Carrington, M. Cook, R. Hobbs, J. Osborne, T. Powell, R. Salisbury and T. des Vallières), pp. 649–655. London, UK: Society for Underwater Technology.

Poulos, H. & Hull, T. (1989). The role of analytical geomechanics in foundation engineering. In *Foundation engineering: Current principles and practices*, Vol. 2, pp. 1578–1606. Reston, VA, USA: ASCE.

Skaare, B., Nielson, F. G., Hanson, T. D., Rune, Y., Havmøller, O. & Rekdal, A. (2015). Analysis of measurements and simulations from the Hywind Demo floating wind turbine. *Wind Energy* **18**, No. 6, 1105–1122.

Zhu, F., O'Loughlin, C. D., Bienen, B., Cassidy, M. J. & Morgan, N. (2018). The response of suction caissons to long-term lateral cyclic loading in single layer and layered seabeds. *Géotechnique* **68**, No. 8, 729–741, https://doi.org/10.1680/jgeot.17.P.129.